PSTPIP2 deficiency in mice causes osteopenia and increased differentiation of multipotent myeloid precursors into osteoclasts

Violeta Chitu,[1] Viorel Nacu,[1] Julia F. Charles,[2,3] William M. Henne,[4] Harvey T. McMahon,[5] Sayan Nandi,[1] Halley Ketchum,[1] Renee Harris,[1] Mary C. Nakamura,[2,3] and E. Richard Stanley[1]

[1]Department of Developmental and Molecular Biology, Albert Einstein College of Medicine, Bronx, NY; [2]Department of Medicine and Rosalind Russell Arthritis Center, University of California, San Francisco, San Francisco, CA; [3]Medical Service, Veterans Administration Medical Center, San Francisco, CA; [4]Weill Institute for Cell and Molecular Biology and Department of Molecular Biology and Genetics, Cornell University, Weill Hall, Ithaca, NY; and [5]Medical Research Council Laboratory of Molecular Biology, Hills Road, Cambridge, United Kingdom

Missense mutations that reduce or abrogate myeloid cell expression of the F-BAR domain protein, proline serine threonine phosphatase-interacting protein 2 (PSTPIP2), lead to autoinflammatory disease involving extramedullary hematopoiesis, skin and bone lesions. However, little is known about how PSTPIP2 regulates osteoclast development. Here we examined how PSTPIP2 deficiency causes osteopenia and bone lesions, using the mouse PSTPIP2 mutations, *cmo,* which fails to express PSTPIP2 and *Lupo,* in which PSTPIP2 is dysfunctional. In both models, serum levels of the pro-osteoclastogenic factor, MIP-1α, were elevated and CSF-1 receptor (CSF-1R)–dependent production of MIP-1α by macrophages was increased. Treatment of *cmo* mice with a dual specificity CSF-1R and c-Kit inhibitor, PLX3397, decreased circulating MIP-1α and ameliorated the extramedullary hematopoiesis, inflammation, and osteopenia, demonstrating that aberrant myelopoiesis drives disease. Purified osteoclast precursors from PSTPIP2-deficient mice exhibit increased osteoclastogenesis in vitro and were used to probe the structural requirements for PSTPIP2 suppression of osteoclast development. PSTPIP2 tyrosine phosphorylation and a functional F-BAR domain were essential for PSTPIP2 inhibition of TRAP expression and osteoclast precursor fusion, whereas interaction with PEST-type phosphatases was only required for suppression of TRAP expression. Thus, PSTPIP2 acts as a negative feedback regulator of CSF-1R signaling to suppress inflammation and osteoclastogenesis. (*Blood*. 2012;120(15):3126-3135)

Introduction

The combination of chronic immune activation and musculoskeletal tissue damage is the hallmark of rheumatic diseases.[1] Osteolytic lesions coupled with skin and/or joint inflammation occur in several rheumatic conditions, such as rheumatoid arthritis, psoriatic arthritis, and chronic recurrent multifocal osteomyelitis (CRMO).[1,2] Thus, an understanding of the pathophysiologic mechanisms underlying rheumatic disease requires the identification of the molecular pathways that simultaneously regulate inflammation and bone homeostasis.

Osteoclasts are bone-resorbing multinucleated giant cells of myeloid origin. Receptor activator of nuclear factor κB ligand (RANKL) and colony stimulating factor-1 (CSF-1) are necessary and sufficient for osteoclast differentiation from monocytic precursor cells in vivo and in vitro.[3-5] CSF-1 modulates multiple steps of osteoclastogenesis, including proliferation of mononuclear OC precursors (OCP), their differentiation and their fusion. In synergy with RANKL, CSF-1 also stimulates the expression of several osteoclast-specific genes including RANK, components of RANK signaling pathways and tartrate-resistant acid phosphatase (TRAP).[6-9]

Proline serine threonine phosphatase-interacting protein 2 (PSTPIP2), also known as macrophage F-actin–associated and tyrosine phosphorylated protein (MAYP), is a Fes CIP4 homology domain (FCH) and Bin/Amphiphysin/Rvs (BAR; F-BAR) protein, predominantly expressed in the myeloid lineage.[10] It is rapidly tyrosine phosphorylated after activation of CSF-1 receptor (CSF-1R),[10-14] and exhibits reduced phosphorylation in mast cells in which c-Kit is inhibited.[12] The mouse *Pstpip2* missense mutations, chronic multifocal osteomyelitis (*cmo*), L98P (*Pstpip2*$^{cmo/cmo}$), and *Lupo* I282N (*Pstpip2*$^{Lupo/Lupo}$) lead to similar autoinflammatory diseases, both characterized by splenomegaly, skin necrosis, and aseptic osteomyelitis. These diseases resemble CRMO and psoriatic arthritis in man.[11,14-17] The mutations result in complete (*cmo*) or partial (*Lupo*) PSTPIP2 protein deficiency, indicating that PSTPIP2 has anti-inflammatory activity.[11,14] Histologic studies of the *cmo* mice showed osteoclast-mediated bone resorption at sites of inflammation in caudal vertebrae,[15,17] and cultured *cmo* bone marrow cells exhibited increased vitamin D_3–induced osteoclastogenic responses.[17] However, the molecular bases of these phenotypes were not elucidated.

In this study, we show that, in addition to the bone erosive disease, PSTPIP2 deficiency leads to generalized osteopenia and CSF-1R–dependent elevation of osteoclast precursors and of serum MIP-1α. Absence of PSTPIP2 causes a cell autonomous defect favoring osteoclastogenesis from multipotent myeloid precursors. In addition, we demonstrate that several distinct molecular interactions of PSTPIP2 are required for suppression of osteoclast differentiation at different stages. Although CSF-1 and RANKL

Submitted April 23, 2012; accepted August 7, 2012. Prepublished online as *Blood* First Edition paper, August 24, 2012; DOI 10.1182/blood-2012-04-425595.

The online version of this article contains a data supplement.

The publication costs of this article were defrayed in part by page charge payment. Therefore, and solely to indicate this fact, this article is hereby marked "advertisement" in accordance with 18 USC section 1734.

positively regulate osteoclastogenesis,[6-9] our results demonstrate that CSF-1R–regulated PSTPIP2 tyrosine phosphorylation is required for suppression of osteoclastogenesis, indicating that PSTPIP2 normally plays a negative feedback role.

Methods

Antibodies and reagents

The dual specificity inhibitor, PLX3397, was a gift from Plexxikon. RANKL was purchased from Cell Sciences. Anti-CD117–FITC, anti-CD11b–APC, anti-CD16/CD32–PE, anti-Ly6C–FITC, anti-CD11c–FITC, anti-CD48–FITC, anti-CD34–FITC, anti-CD150–PE, and streptavidin-PE were from BD Pharmingen. Pacific Blue anti–Sca-1, anti-CD49b–APC, anti-Ly6G–PerCP, and anti-CD3–FITC were from BioLegend. Anti-B220–PE-Cy5, anti–CD4-PE–Cy5, anti–CD19-PE–Cy5, anti-CD8–PE-Cy5, anti-CD127PE, anti-CD117–APC, biotinylated-AFS98, and anti-Thy1.1–FITC were from eBioscience. CSF-1 was a gift from Chiron Corporation. Unless otherwise specified, all other reagents were purchased from Sigma-Aldrich.

Mice and genotyping

Pstpip2$^{cmo/cmo}$ BALB/cAnPt and wild-type (WT) BALB/cByJ mice (The Jackson Laboratory) and *Pstpip2*$^{Lupo/Lupo}$ C3HeB/FeJ and WT C3HeB/FeJ mice (Ingenium Pharmaceuticals) were maintained under specific pathogen-free conditions in a barrier facility of the Albert Einstein College of Medicine Animal Institute, which approved the mouse breeding and study protocols. In addition, this study was conducted in accordance with the Declaration of Helsinki. *Pstpip2* mutation genotyping was performed by PCR amplification and sequencing as described.[11,14]

Treatment with PLX3397 and scoring of inflammation

Treatment with PLX3397 or control chow was initiated at 5 weeks of age, before the onset of clinical disease. Inflammation was scored weekly by visual examination using the following criteria: (1) Skin for ears: 1 point for each of the following: erythema, edema, tissue hardening, or necrosis. Score doubles for bilateral symptoms. For body hair loss: localized, 1 point; general, 2 points. (2) Paws: 1 point for each of the following: bulbous toe, local signs of erythema, edema, tissue hardening, or necrosis. Score doubles if symptoms are generalized or bilateral. (3) Tails: 1 point for each tail kink and 1 point for swelling or redness.

Micro-computed tomography

After serial fixation in 4% phosphate-buffered formaldehyde and 70% ethanol, bones were scanned by high resolution micro-CT. Imaging was performed using vivaCT 40 with a voxel size of 10.5 μm (see Figure 1), and with μCT 35 (both Scanco Medical) with a voxel size of 7 μm (see Figure 3). Structural parameters were calculated using Scanco Medical Version 6 software on an area extending 2.1 mm from the metaphysis for trabecular bone and 0.6 mm at the femoral midshaft. Analysis was performed using segmentation values of 0.8/1/375 for cortical data and 0.8/1/250 and 0.8/1/275 for trabecular data in Figures 1 and 3, respectively. Paws, tail, and/or spine were imaged with vivaCT40, voxel size 15 μm, segmentation values of 0.7/1/425 (see Figure 1), or with μCT 35, voxel size 12.5 μm, segmentation values of 0.8/1/300 (see Figure 3).

Histologic and ultrastructural analysis

For TRAP staining, mice were anesthetized and perfused with periodate-lysine-paraformaldehide-glutaradehyde (PLPG) fixative by injection of the fixative in the heart.[18] Tissues were dissected, further fixed by immersion in PLPG, and embedded in paraffin. Sections stained for TRAP and counter-stained with hematoxylin were analyzed by light microscopy, using a Zeiss AxioSkop 2 (Carl Zeiss Microscopy) equipped with a Plan Neofluar objective 2.5×/0.075 NA and the images collected using Axiovision 4.1 software. For electron microscopic studies, 4-month-old mice were perfused with 2% paraformaldehyde and 2.5% glutaraldehyde in cacodylate buffer, pH 7.4. Tail vertebrae were fixed and processed as previously described.[19] Sections were examined using a JEOL 1200EX transmission electron microscope (JEOL) and representative regions were photographed. Images were cropped and adjusted for brightness, contrast, and color saturation using Adobe Photoshop Elements 2.0.

Analysis of osteoclast and myeloid precursors by flow cytometry

Bone marrow cells, splenocytes and blood were collected from mice subjected to the indicated treatments. After red blood cell lysis and Fc receptor blocking, cells were labeled with anti-CD117–FITC, anti-CD11b–APC, biotinylated Rat IgG 2a anti–CSF-1R AFS98, and streptavidin-PE. Bone marrow populations containing myeloid and osteoclast precursors were identified as described,[8,20] and analyzed or sorted using a BD-LSR II, or a BDFACS Aria I cell sorter (Becton Dickinson), respectively. Spectral overlaps between fluorophores corrected by electronic compensation. FACS data were analyzed using FlowJo Version 8.8.6 software (TreeStar).

Osteoclast differentiation and precursor proliferation

Osteoclasts were generated from bone marrow cells extracted from the femurs of WT or *Pstpip2*$^{cmo/cmo}$ mice, or from FACS-sorted osteoclast precursors, in triplicate cultures containing 30 ng/mL M-CSF and 100 ng/mL RANKL, as previously described.[8,21] Cells were fixed at the indicated times and stained for TRAP as described elsewhere.[22] Cells were examined under an Olympus CK2 inverted microscope (Olympus) equipped with an Olympus 10× objective, 0.25 NA. Digital images were acquired using a Kodak DC290 camera equipped with an Optem (1×) microscope adaptor and the Kodak camera digital software. Images were cropped and adjusted for brightness, contrast, and color balance using Photoshop Elements 2.0. TRAP activity was also determined in cultures grown in 96-well plates as described.[23]

Bone resorption assay

Bone marrow cells were plated on whale dentine slices (Immunodiagnostic Systems) for 6 days in the presence of 30 ng/mL CSF-1 and 100 ng/mL RANKL with a change of media at day 3. Cells were fixed in 4% paraformaldehyde for 20 minutes at room temperature and stained for TRAP. In some experiments, cells were removed by sonication in 0.25M ammonia hydroxide, the resorptive pits stained with toluidine blue and the stained dentin slices analyzed by light microscopy using a Zeiss STEMI (Carl Zeiss Microscopy) and IPLab 4.0.8 software. The quantitation of resorption was performed using ImageJ Version 1.4lo software. Images were cropped and adjusted for brightness, contrast, and color balance using Photoshop Elements 2.0. The same methods were applied to dentine slice implants.

Dentine implantation, PLX3397 treatment, and measurement of serum markers for inflammation

Dentine discs (Immunodiagnostic Systems) were incubated overnight in α-MEM with 10% FCS, 30 ng/mL CSF-1, and 100 ng/mL RANKL and implanted bilaterally in the gluteus maximus of mice under general anesthesia. Mice were euthanized at the indicated times and the discs were removed and stained for TRAP or resorption pits as described under "Bone resorption assay." Blood was collected at the indicated times and sera were screened for cytokine production using multiplexed beadlyte mouse cytokine kits (Millipore) as described[14] or using the mouse IL-6 ELISA Ready-SET-Go kit (eBioscience). Osteoclast precursors in blood, bone marrow, and spleen were analyzed by flow cytometry as described under "Analysis of osteoclast and myeloid precursors by flow cytometry."

Generation of osteoclast precursor cell lines and retroviral reconstitution of PSTPIP2 expression

Early c-Kit^{+} Mac-1^{lo} c-Fms^{lo} osteoclast precursors were purified by FACS sorting and immortalized using a retroviral construct encoding SV40 large

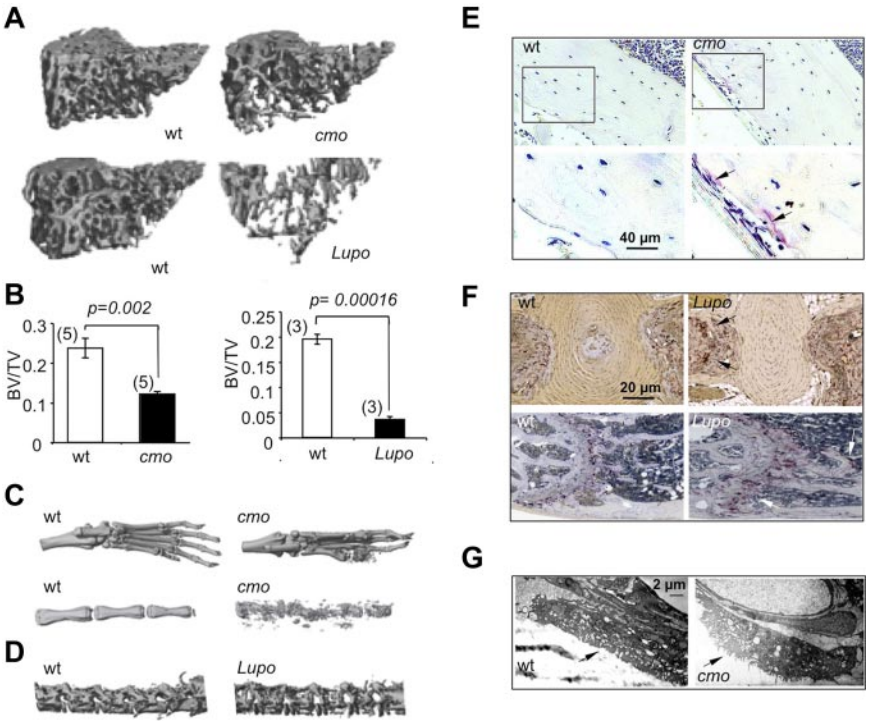

Figure 1. Diseased PSTPIP2-deficient mice are osteopenic and have erosive bone lesions that are associated with increased osteoclast numbers and activity. (A) Representative 3D reconstructions of trabecular areas of proximal tibias from PSTPIP2-deficient 3.5-month-old *cmo* and 3-month-old *Lupo* mice (right panels) and their corresponding WT control mice (left panels). (B) Quantitative micro-CT analyses of 3-month-old female mice showing that, compared with WT controls (white bars), PSTPIP2-deficient mice (black bars) have decreased proximal tibia bone volume to total volume (BV/TV). Figures in parentheses indicate the numbers of mice in each group. (C) Representative images of paws and proximal tails from *cmo* and WT control mice. Erosive bone lesions are seen on micro-CT reconstructions of paws and tails of diseased *cmo* mice. (D) Lumbar vertebrae from *Lupo* mice demonstrate osteopenia. (E) Increased TRAP staining in sections of femoral cortex of *cmo* compared with WT controls. Bottom panels are higher magnifications of the boxed regions in the top panels. (F) TRAP staining of tail vertebrae (top panels) and proximal femurs (bottom panels) of *Lupo* mice and WT controls. Arrows indicate TRAP$^+$ osteoclasts. (G) Electron micrographs of vertebral osteoclasts. Arrows indicate the ruffled border.

T antigen as described.[14] PSTPIP2 mutants were prepared using a QuikChange site-directed mutagenesis kit (QIAGEN) and the presence of the desired mutations was confirmed by DNA sequencing. PSTPIP2 expression was reconstituted by MSCV-IRES-GFP retroviral transduction as described.[24]

Biochemical characterization of PSTPIP2 mutants

For lipid binding studies, PSTPIP2 was cloned in pGEX-6-P1, and expressed in *Escherichia coli* as GST-fusion protein. GST-PSTPIP2 was purified by affinity chromatography and the GST tag was removed by digestion with PreScission protease. WT PSTPIP2 and mutants were then tested for phospholipids binding ability using PIP strips (Echelon Biosciences). Cell stimulation, immunoprecipitation and Western Blotting were performed as described.[24]

PSTPIP2 in vitro tubulation assay and CD Spectroscopy

Folch fraction I (Sigma-Aldrich) liposomes were prepared by classic dehydration-rehydration protocols. Lipids were prepared in a 1:1 chloroform: methanol mix and dried in glass tubes under Argon gas. Liposomes were rehydrated in buffer (150mM NaCl, 20mM HEPES pH 7.4, 2.5mM DTT), sonicated, and filtered through 0.8-μm pore diameter polycarbonate filters (Whatman) to a final concentration of 1 mg/mL. Purified PSTPIP2 was mixed at 5 to 12μM with 0.5 mg/mL liposomes (final concentrations) and allowed to incubate for 30 minutes, and then adhered to glow-discharged carbon-coated TEM grids (Agar Scientific) for 1 minute. Samples were briefly dehydrated, negative stained with 2% uranyl acetate, and then briefly washed with water and imaged. All samples were imaged on a PW6010/20 EM2055 transmission electron microscope at 80 kV (Philips).

To assess protein folding, reconstituted PSTPIP2 proteins were resuspended in 5mM HEPES pH 7.4, 150mM NaCl. CD spectra were obtained using a Jobin Yvon CD6 CD spectrophotometer (Horiba).

Fluorescence light microscopy

Living *COS-7* cells were cultured on glass-bottom culture dishes (MatTek) in DMEM–GlutaMAX-1 media (Invitrogen) and transfected using GeneJuice (EMD) with plasmids encoding N-terminally EGFP-tagged PSTPIP2 (Clontech). Cells were allowed to express the proteins overnight before imaging. For imaging, cells were placed in a temperature-controlled chamber heated to 37°C that was installed on a fully motorized inverted light microscope Eclipse TE-2000 (Nikon) equipped with a CSU-X1 spinning disk confocal unit (UltraVIEW VoX) and four 50-mW solid-state lasers. Living cells were imaged through a 60× lens (Plan Apochromat VC, 1.4 NA, Nikon). The system was operated through Volocity 5.0 (Improvision) software. Video images were acquired at 2 frames/second. Images were obtained with a cooled EMCCD camera (9100-02; Hamamatsu).

Statistics

Significance was tested using the 2-tailed Student *t* test.

Results

Diseased PSTPIP2-deficient *Pstpip2*$^{cmo/cmo}$ mice are osteopenic and have erosive bone lesions

Diseases characterized by erosive arthritis frequently manifest generalized bone loss.[1] To determine whether this was also a characteristic of the autoinflammatory and erosive disease seen in PSTPIP2-deficient mice, we examined trabecular and cortical bone parameters by microcomputed tomography (micro-CT). Proximal tibia trabecular bone was significantly decreased in diseased female *cmo* and *Lupo* mice, compared with age-and sex-matched WT controls (Figure 1A-B). Similar differences were seen at the distal femur and in cohorts of diseased male mice compared with WT controls (data not shown). Consistent with previous reports demonstrating osteolysis in the caudal vertebrae,[15,17] representative 3D micro-CT reconstructions of paws and proximal tails of diseased *cmo* mice show that they developed erosive bone lesions at sites of inflammation (Figure 1C). In addition, although *Lupo* mice did not develop kinked tails, significant bone erosion was detected in the lumbar region of the spine (Figure 1D bottom panels). Thus, as observed in psoriatic or rheumatoid arthritis,[1] the

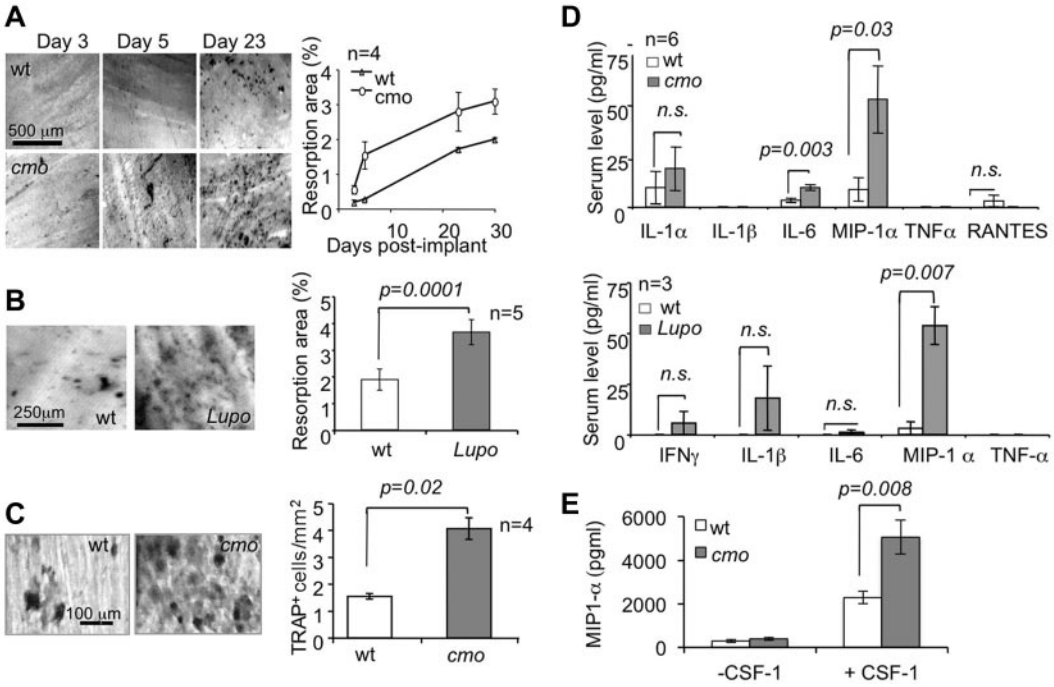

Figure 2. PSTPIP2 deficiency promotes osteoclast development and MIP-1α production in vivo. (A) Toluidine blue staining (left panels) and quantitation (right panel) of the resorption pits on dentine implants removed at the indicated times after surgery. (B) Resorption pits (left panels) and quantitation (right panel) of dentine resorption at day 10 postimplant. (C) TRAP staining of dentine implants (left panels) and quantitation of the density (right panel) of TRAP$^+$ cells on implants removed at day 5. (D) Serum levels of pro-osteoclastogenic factors in 6-month-old *cmo* (top panel) and 3-month-old *Lupo* (bottom panel) mice and WT controls at day 8 after surgery. (E) MIP-1α production by macrophages after a 24-hour incubation in medium with or without 120 ng/mL CSF-1. Data ± SEM; n indicates number of mice per group; and ns, not significantly different ($P > .05$).

inflammatory diseases of PSTPIP2-deficient mice lead to both localized bone erosions and generalized bone loss.

Increased osteoclast density and osteoclast activation in *cmo* mice

Histologic analysis revealed increased TRAP staining in the long bones of both *cmo* (Figure 1E) and *Lupo* mice (Figure 1F), indicative of increased osteoclast formation. Furthermore, electron microscopic examination of osteoclast morphology revealed that compared with WT mice, tail vertebrae sections obtained from *cmo* mice contained osteoclasts exhibiting prominent ruffled borders (Figure 1G), indicative of active bone resorption.[25]

PSTPIP2-deficient mice exhibit accelerated and enhanced resorption of dentine disc implants and increased serum levels of the pro-osteoclastogenic factor MIP-1α

To test the impact of PSTPIP2-deficiency disease in mice on osteolytic responses in vivo, we performed intramuscular dentine disc implantation in PSTPIP2-deficient and WT mice. Both *cmo* (Figure 2A) and *Lupo* mice (Figure 2B) display more extensive osteolytic responses against the dentine implants than WT controls. This phenotype is associated with increased formation of TRAP$^+$ cells on the surface of the implant (Figure 2C) and with increased circulating levels of MIP-1α, without significant elevation of other factors involved in osteoclast differentiation or osteoclast precursor mobilization, including IL-1α, IL-1β, TNF-α, or RANTES (Figure 2D). Although circulating levels of another pro-osteoclastogenic factor, IL-6, were significantly increased in *cmo* mice (Figure 2D), they were normal in 3-month-old *Lupo* mice (Figure 2D bottom panel). To confirm this, we carried out additional measurements of serum IL-6, using the more sensitive ELISA assay. There was no significant difference between serum IL-6 levels of WT and *Lupo* mice at either 3 months (WT 6.1 ± 2.6 pg/mL, n = 7; *Lupo*, 7.9 ± 2.1 pg/mL, n = 12; $P = .62$) or 8 months (WT 7.4 ± 3.4 pg/mL, n = 3; *Lupo*, 10.9 ± 2.4 pg/mL, n = 9, $P = .45$) of age. The significant loss of trabecular bone in 3-month-old *Lupo* mice (Figure 1B), in the absence of elevated IL-6 suggests that IL-6 is not a major contributor to the osteopenic phenotype of PSTPIP2-deficient mice. MIP-1α production by macrophages was dependent on CSF-1R signaling and was significantly higher in the absence of PSTPIP2 expression (Figure 2E), suggesting that PSTPIP2 negatively controls CSF-1–stimulated MIP-1α production.

Inhibition of CSF-1R and c-Kit signaling reduces inflammation, the availability of OC precursors and attenuates disease in *cmo* mice

Stem cell factor (c-Kit ligand) and CSF-1 together regulate the proliferation of multipotent hematopoietic progenitor cells and their myeloid differentiation.[26] Osteoclast precursors are substantially enriched among the c-Kit$^+$ c-Fms^{lo} Mac1^{lo} multipotent myeloid precursor (early osteoclast precursor, EOCP) and the c-Kit$^+$ c-Fms^{hi} Mac1^{lo} bipotent (monocyte/osteoclast) precursor (late osteoclast precursor, LOCP) fractions of the bone marrow.[8] We observed that both *cmo* bone marrow and spleen contain increased numbers of these precursors (Figure 3H). To test whether CSF-1 and c-Kit–dependent expansion of OCP significantly contributes to the inflammation and osteopenia in *cmo* mice, we administered PLX3397, a CSF-1R/c-Kit dual-specificity inhibitor,[27] to asymptomatic *cmo* mice and examined its effect on disease development. PLX3397 significantly attenuated autoinflammatory disease (Figure 3A), decreasing the erosive bone lesions in tails and paws (Figure 3B-C) and the levels of circulating MIP-1α (Figure

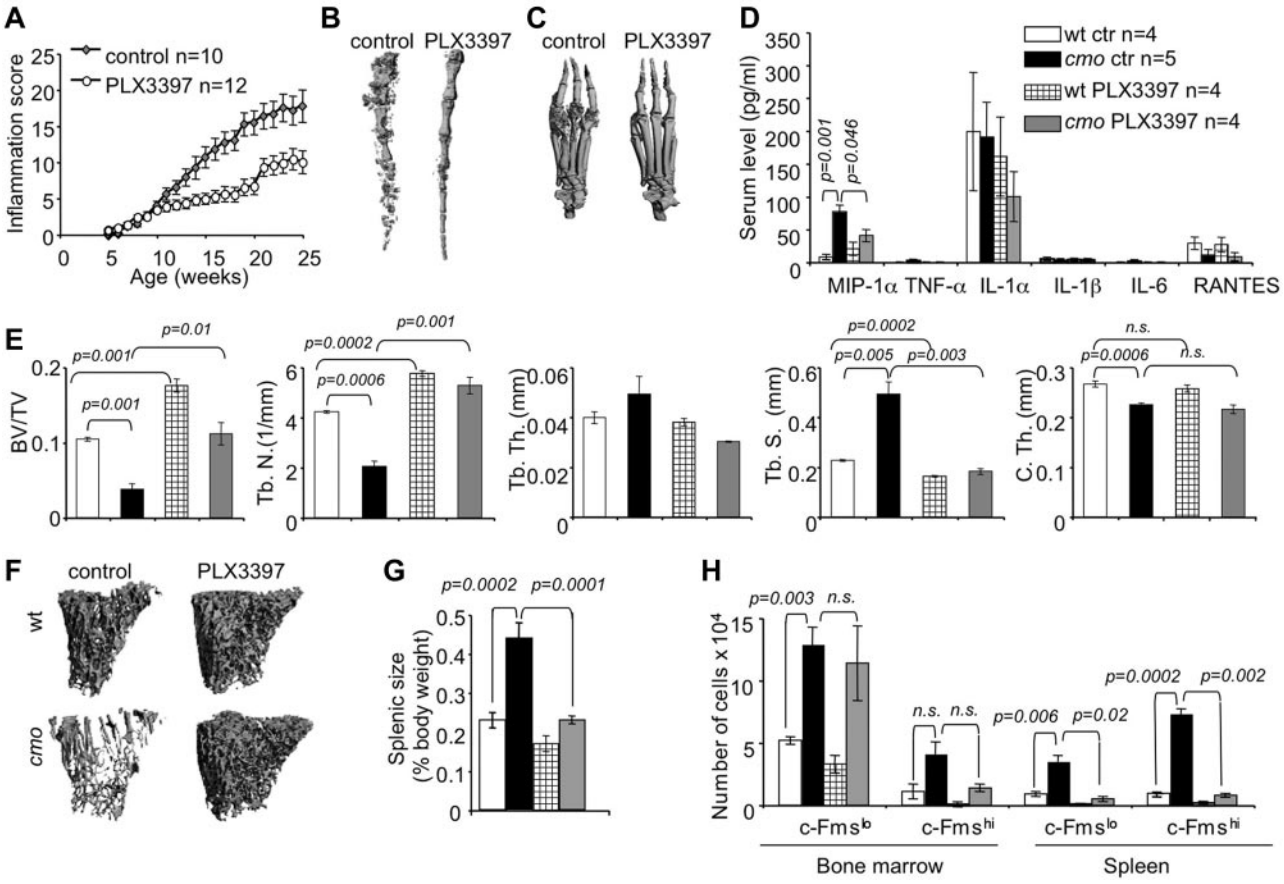

Figure 3. Inhibition of myelopoiesis using a dual c-Fms/c-Kit inhibitor attenuates inflammation and bone destruction in *cmo* mice. (A) Time course of disease progression in *cmo* mice receiving the c-Fms/c-Kit inhibitor, PLX3397 (PLX), or control chow. Treatment was started at 5 weeks of age, before the onset of clinical symptoms and continued up to ~ 8 months of age (WT, 252 ± 18 and *cmo* 248 ± 19 days), at which time the mice were euthanized and analyzed. (B-C) Micro CT reconstruction of distal tails (B) and hind paws (C) of PLX-treated and control *cmo* mice. (D) PLX treatment decreases circulating MIP-1α in *cmo* mice. (E) Quantitative bone parameters of PLX-treated and control *cmo* and WT mice. (F) Micro CT reconstructions of proximal tibiae. (G-H) PLX treatment of *cmo* mice prevents splenomegaly (G) and the expansion of splenic OCP (H). Scale bars, 100 μm. Data ± SEM, n ≥ 3.

3D) in *cmo* mice. Moreover, PLX3397 completely abrogated the generalized trabecular bone loss seen in diseased *cmo* mice and also increased trabecular bone in WT mice (Figure 3E-F). However, there was no effect of PLX3397 treatment on cortical thickness in either WT or *cmo* mice (Figure 3E).

The extramedullary hematopoiesis with splenomegaly (Figure 3G) and the expansion of splenic EOCP, LOCP (Figure 3H), myeloid precursors (Figure 4A), granulocytes, monocytes, and macrophages (Figure 4B) were also inhibited by PLX3397. In contrast, PLX3397 had no effect on early myelopoiesis in bone marrow (Figure 3H and data not shown). These data suggest that increased CSF-1R and c-Kit signaling plays a central role in the development of *cmo* autoinflammatory disease by promoting myelopoiesis in the spleen.

PSTPIP2 deficiency leads to increased differentiation of c-Kit$^+$ c-fms^{lo} Mac1^{lo} EOCP

Because the frequencies of bone marrow OC precursors were comparable in WT and *cmo* mice, yet osteoclasts developed faster in *cmo* bone marrow cultures than in WT cultures (supplemental Figure 1, available on the *Blood* Web site; see the Supplemental Materials link at the top of the online article), we determined whether PSTPIP2 deficiency enhanced the ability of OC precursors to differentiate by assessing the ability of isolated multipotent c-Kit$^+$ c-Fms^{lo} Mac1^{lo} EOCP and more mature c-Kit$^+$ c-Fms^{hi} Mac1^{lo} LOCP to acquire TRAP expression and to fuse into osteoclasts in vitro, in the presence of CSF-1 and RANKL. The c-Kit$^+$ c-Fms^{hi} Mac1^{lo} LOCP fraction isolated from *cmo* or WT bone marrow exhibited comparable ability to form osteoclasts (Figure 5A top panels and B). In contrast, the c-Kit$^+$ c-Fms^{lo} Mac1^{lo} EOCP fraction isolated from *cmo* mice exhibited an increased ability to generate TRAP+ cells and formed larger osteoclasts in vitro compared with the same fraction from WT mice (Figure 5A bottom panels and B). Similar results were obtained using EOCP isolated from *Lupo* mice (Figure 5C). These data indicate that PSTPIP2 negatively regulates the differentiation of c-Kit$^+$ c-Fms^{lo} Mac1^{lo} EOCP.

The Lupo mutation (I282N) impairs the function of the PSTPIP2 F-BAR domain and PSTPIP2 stability

The *cmo* mutation (L98P) is located within the predicted F-BAR domain, which mediates PSTPIP2 interaction with membrane phospholipids and promotes membrane curvature,[28] whereas the *Lupo* mutation (I282N) is located adjacent to the F-BAR domain. In contrast to the *cmo* mutation which leads to absence of detectable PSTPIP2 protein expression,[14] the *Lupo* mutation leads to partial protein deficiency.[11] However, I282 is highly conserved in F-BAR proteins and molecular modeling predicts that substitution of the hydrophobic I282 with a polar residue (Asn) destabilizes the 3D structure by impeding the contact of the unstructured C-terminus

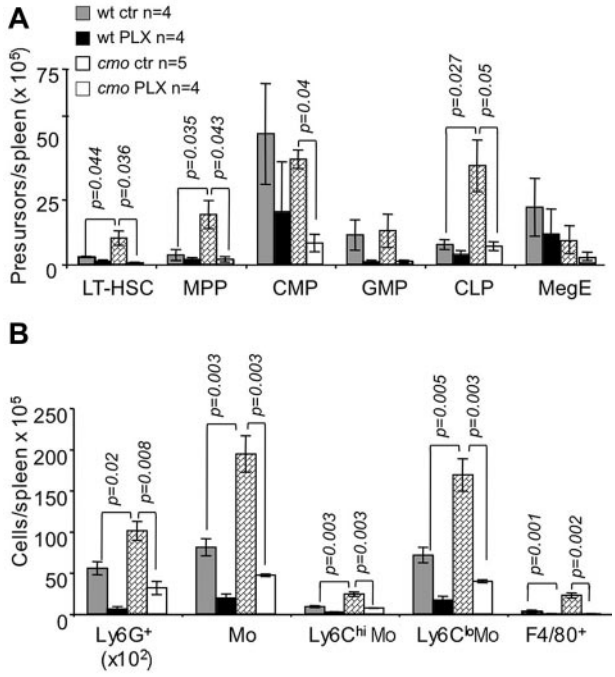

Figure 4. The dual specificity c-Fms and c-Kit inhibitor, PLX3397, suppresses extramedullary hematopoiesis in *cmo* mice. PLX3397 prevents the expansion of both early hematopoietic precursors (A) and myeloid cells (B) in spleen. Data ± SEM; n indicates number of mice/group; and ns, not significant ($P > .05$).

with a hydrophobic groove (supplemental Figure 2A and Henne et al[29]). Thus, we investigated the impact of the *Lupo* mutation on the structure and function of PSTPIP2 in membrane tubulation experiments, which are a standard measure of the membrane-bending activity of BAR and F-BAR domain-containing proteins.[29-31] The PSTPIP2 I282N mutation did not significantly affect PSTPIP2 folding in solution (supplemental Figure 2B), nor the ability of PSTPIP2 to tubulate liposomes in vitro (Figure 6A). We therefore examined the formation and stability of tubules formed in cells overexpressing the WT or mutant PSTPIP2, a condition that permits analysis of tubule turnover, as well as interactions of PSTPIP2 with other cellular proteins. PSTPIP2 was followed in these experiments by tagging the N-terminus with GFP, as N-terminal tagging does not affect PSTPIP2 activities in macrophages.[24] Membrane tubules induced by the overexpression of the I282N mutant in *COS-7* cells were unstable compared with those formed by WT PSTPIP2 (Figure 6B). In general, tubules generated by the I282N mutant were less abundant and typically broke at one end, indicated by a quick loss of fluorescence down the axis of the tubule (Figure 6C). This suggested a fast depolymerization of the tubule PSTPIP2 I282N coat. EGFP-PSTPIP2 I282N (Figure 6D), but not EGFP-PSTPIP2 WT, also appeared to aggregate in transfected cells, forming fluorescent densities throughout the cytoplasm. Aggregates were closely associated with membrane tubules, and some appeared tethered to the tubules in live cell imaging (Figure 6D), suggesting that they are generated at sites of high PSTPIP2 concentration (ie, tubules). These observations indicate that the I282N mutation significantly affects both the ability of PSTPIP2 to stabilize membrane curvature, as well as the stability of PSTPIP2 itself. They also demonstrate that although residual PSTPIP2 is expressed in *Lupo* mice, it is dysfunctional.

Distinct steps of osteoclastogenesis are negatively regulated by PSTPIP2 tyrosine phosphorylation, membrane interactions, or PEST-type phosphatase binding

To better understand how PSTPIP2 modulates osteoclast differentiation, we generated an immortalized c-Kit$^+$ c-Fms^{lo} Mac1^{lo} OC precursor *cmo* cell line (cmoOCP) that failed to express endogenous PSTPIP2 protein. We then reconstituted PSTPIP2 expression in these cells by retroviral transduction of WT PSTPIP2 (P2WT; Figure 7A) and mutants, an R116Q, K117Q mutant unable to interact with membrane phospholipids (KRQ; Figure 7B), a W232A mutant unable to interact with PEST-type phosphatases (WA; Figure 7C), or a mutant that eliminates CSF-1R–stimulated PSTPIP2 tyrosine phosphorylation (Y2F; Figure 7D). The levels of expression of the PSTPIP2 mutants in cells were only slightly lower than the expression of WT PSTPIP2 (Figure 7E), indicating that these mutations did not significantly impair PSTPIP2 stability. After 5 days of culture in CSF-1 and RANKL, *cmo*OCPs transduced with the vector develop into large multinucleated TRAP$^+$ osteoclast-like cells (OCLC). In contrast, in cultured *cmo*OCPs expressing WT PSTPIP2, the development of OCLCs was dramatically suppressed (Figure 7F). The WA mutant also suppressed OCLC development, but was less effective at suppressing TRAP

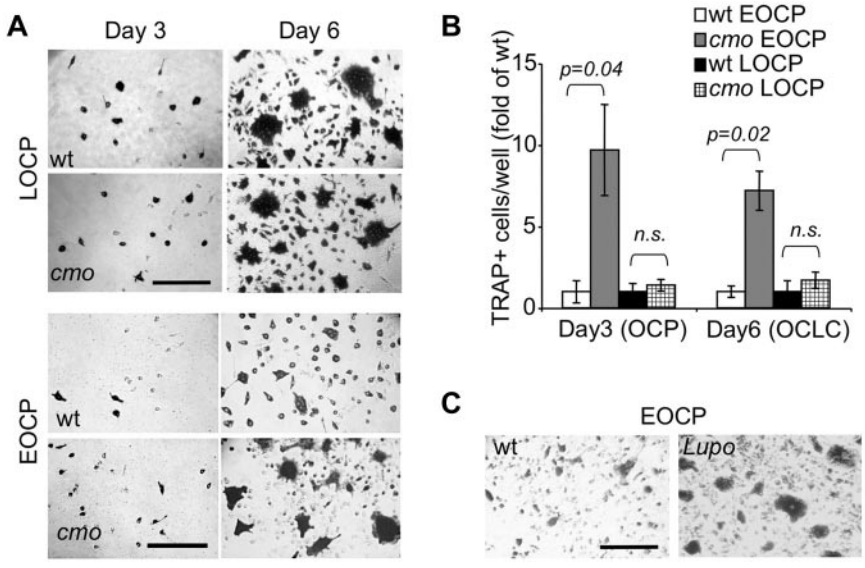

Figure 5. PSTPIP2 deficiency enhances osteoclast development from purified precursors. (A) TRAP staining of c-Kit$^+$ c-Fms^{hi} Mac-1^{lo} (LOCP) and c-Kit$^+$ c-Fms^{lo} Mac-1^{lo} (EOCP) osteoclast precursor cultures at day 3 and day 6 of CSF-1 and RANKL-induced osteoclast differentiation in vitro. (B) Quantitation of TRAP$^+$ mononuclear OCP (day 3) or OCLC cells (day 6) shown in panel A. Data ± SEM from 3 independent experiments. ns indicates not significant ($P > .05$). (C) Compared with WT controls, cultured *Lupo* EOCP form more TRAP-positive multinucleated osteoclasts.

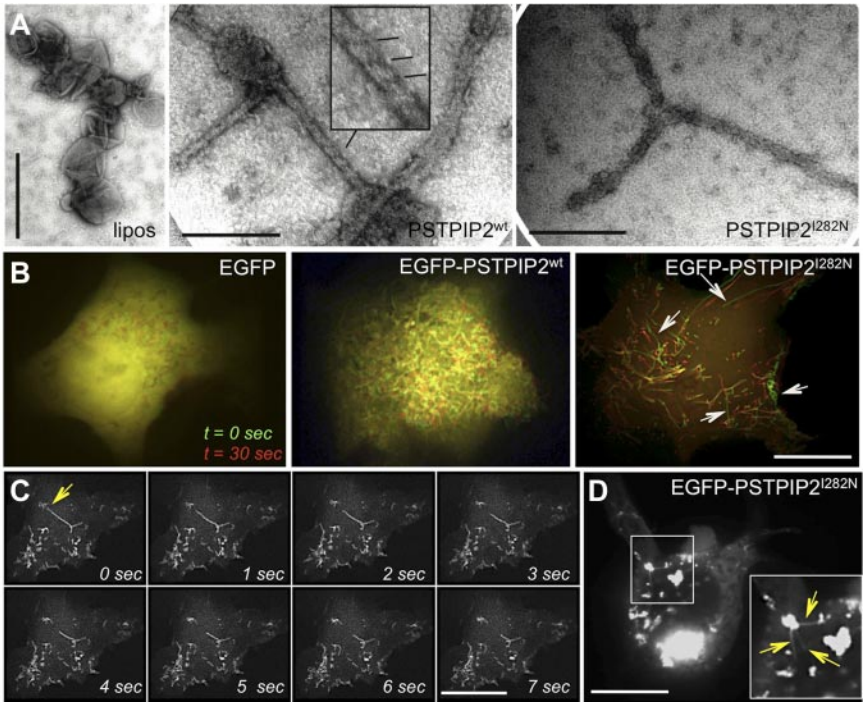

Figure 6. The I282N (*Lupo*) mutation impairs both membrane sculpting by PSTPIP2 and PSTPIP2 stability. (A) Transmission electron micrographs of Folch liposomes (left panel) and liposomes coincubated with WT PSTPIP2 (middle panel) demonstrate that PSTPIP2 typically generates narrow (~ 25-nm diameter) tubules. Striations decorate some portions of the tubules (inset), suggesting a PSTPIP2 repeating scaffold. (Right panel) PSTPIP2 I282N mutation does not attenuate tubulation in vitro. (B) Mutation of I282 affects plasma membrane tubule stability. Pseudocolored fluorescence image of COS-7 cells expressing EGFP alone (left), WT EGFP-PSTPIP2 (middle) or EGFP-PSTPIP2 I282N (right) under live cell imaging. The EGFP fluorescence at time = 0 seconds is displayed in green and in the same cell 30 seconds later, in red. The lengths of PSTPIP2 I282N tubules decrease over time (arrows), whereas WT PSTPIP2 tubules appear stable, as indicated by the colocalization of red and green signals (yellow). Note: movement of tubules during the 30 seconds time frame results in separate green and red images for the same tubule. (C) Time-lapse video frames of live cell imaging of a COS-7 cell expressing EGFP-PSTPIP2 I282N at moderate levels. The arrow in the first frame denotes the site of tubule uncoating. (D) At high expression levels EGFP-PSTPIP2 I282N misfolds into large protein aggregates that are tethered to tubules (inset, arrows). Scale bars, 200 nm in panel A and 20 μm in panels B through D.

expression (Figure 7F-H). In contrast, the Y2F mutant lost the ability to suppress osteoclast development completely (Figure 7F-H). *cmo*OCPs expressing the KRQ mutant had an intermediate phenotype generating fewer, large, multinucleated TRAP$^+$ cells (Figure 7F-H). Interestingly, compared with WT, the KRQ mutant also exhibited reduced tyrosine phosphorylation but, unlike Y2F,

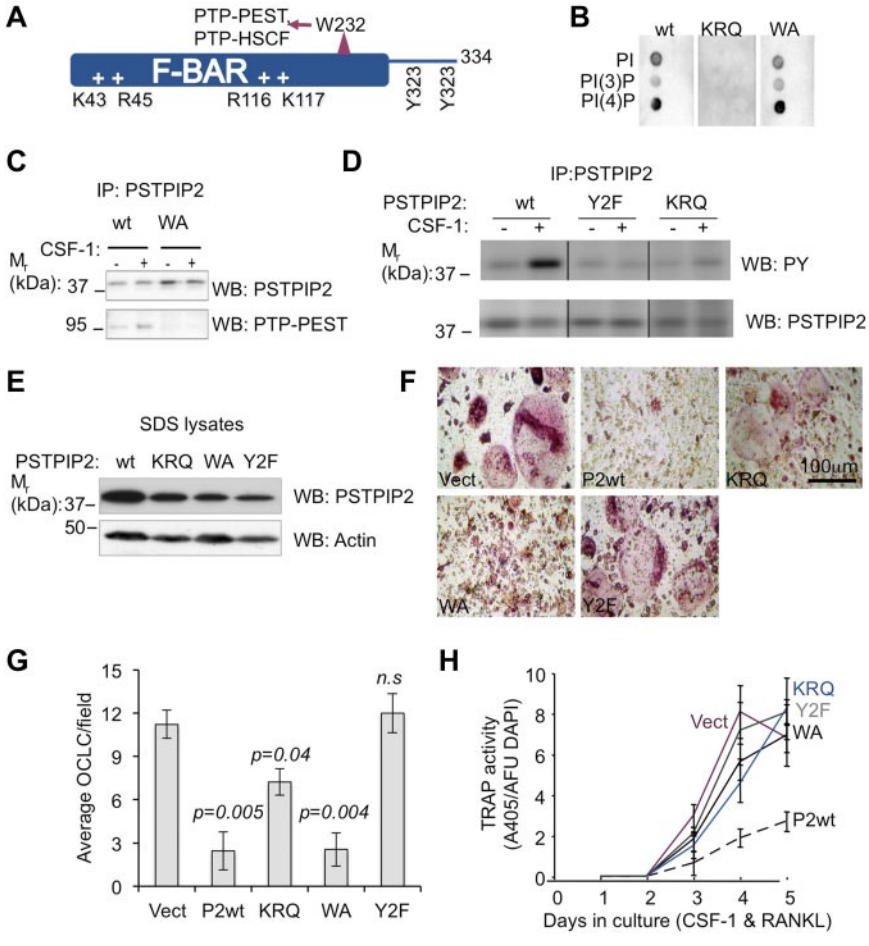

Figure 7. PSTPIP2 tyrosine phosphorylation and interaction with membrane phospholipids are required for PSTPIP2 inhibition of osteoclast differentiation. (A) Predicted structural determinants of PSTPIP2 molecular interactions. (B) Mutation of the conserved cationic residues, R116 and K117 (KRQ), abolishes phospholipid binding. (C) Mutation of W232 to alanine (WA) inhibits PSTPIP2 interaction with PTP-PEST. (D) Mutation of the major tyrosine phosphorylation sites Y323 and Y333 (Y2F) eliminates tyrosine phosphorylation of PSTPIP2 in response to CSF-1 stimulation (middle panel), which is also reduced in CSF-1–stimulated macrophages expressing the KRQ mutant (right panel). Repositioned gel lanes from the same blot are separated by vertical lines. (E) The expression of WT PSTPIP2 and PSTPIP2 mutants was confirmed by Western blotting of SDS cell lysates. Actin indicates loading control. (F) Morphology of day 6 osteoclasts obtained from immortalized *cmo* c-Kit$^+$ Mac-1^{lo} c-Fms^{lo} EOCP retrovirally transduced with vector (Vect), WT PSTPIP2 (P2WT), or the PSTPIP2 mutants described in panels B through E. (G) Quantitation of the number of OCLC per field. (H) Effects of PSTPIP2 deficiency and mutation on TRAP expression. AFU DAPI indicates arbitrary fluorescence units of DAPI-stained cultures. Data ± SEM, n ≥ 3 independent experiments; ns indicates not significant ($P > .05$).

its phosphorylation at CSF-1–regulated sites was increased after stimulation with CSF-1 (Figure 7D right panel). These differences in OC development between cell lines expressing various PSTPIP2 mutants (Figure 7F-H) cannot simply be accounted for by the slight differences in PSTPIP2 expression levels (Figure 7E). For example, the WA mutant was comparable with PSTPIP2 WT in its ability to suppress OCP fusion, whereas the KRQ and the Y2F mutants, expressing PSTPIP2 at levels higher or comparable with those of the WA mutant, were less able to inhibit OCP fusion. We conclude that PSTPIP2 tyrosine phosphorylation and a functional F-BAR domain are essential for its inhibitory actions on TRAP expression and osteoclast precursor fusion, whereas interaction with PEST-type phosphatases (PTP-PEST and PTP-HCSF) is required for suppression of TRAP expression.

Discussion

The identification of changes in bone density associated with chronic immune activation, including autoimmune and autoinflammatory diseases, cancer, and atherosclerosis, has revealed a dynamic interplay between bone and the immune system and has led to the emergence and rapid development of the new field of osteoimmunology.[32,33] In this paper, we focused on the elucidation of the actions of the anti-inflammatory protein PSTPIP2/MAYP[11,14] in osteoclastogenesis. We show that the effects of PSTPIP2 deficiency autoinflammatory disease on the skeletal system are not limited to erosive lesions at sites of inflammation, but lead to generalized osteopenia, resulting from increased osteoclast differentiation. These data demonstrate that PSTPIP2 negatively regulates pathways leading to both inflammation and bone resorption.

PSTPIP2 deficiency causes the elevation of the serum levels of the pro-osteoclastogenic factor, MIP-1α. In response to CSF-1, PSTPIP2-deficient macrophages produce more MIP-1α than WT counterparts (Figure 2E, and Chitu et al[14]). This observation, coupled with the increase in macrophage abundance in PSTPIP2-deficient mice (Figure 4B; Grosse et al[11] and Chitu et al[14]), suggest that macrophages are the major contributor to the elevation of circulating MIP-1α in the mutant mice. Consistent with this, we found that suppression of myelopoiesis using the dual c-Kit/CSF-1R inhibitor, PLX3397 (Figure 3), prevented the elevation of serum MIP-1α and extramedullary hematopoiesis and attenuated disease. PLX3397 also prevented the trabecular bone loss in *cmo* disease. However, in contrast to genetic ablation of the CSF-1R[19] or antibody-mediated ablation of CSF-1[34] in developing mice, there was no effect of PLX 3397 on cortical bone thickness, reflecting the slow turnover rate of cortical bone in adult mice.[35]

MIP-1α is chemotactic for OC precursors in vivo[36] and promotes osteoclastogenesis in vitro, via its actions on both CCR1 and CCR5.[37] CCR1 is the major MIP-1α receptor expressed in preosteoclasts and osteoclasts and is up-regulated during osteoclast differentiation.[36] Studies in CCR1-deficient mice revealed that CCR1 is critical for the mobilization of myeloid precursors and for the enhancement of CSF-1–dependent macrophage colony formation by MIP-1α.[38] Furthermore, blocking MIP-1α signaling, using a CCR1 antagonist, inhibits osteoclastogenesis in vitro.[39] Together, these data suggest that PSTPIP2 deficiency disease results from enhanced CSF-1 signaling leading to overproduction of monocytic lineage cells that subsequently become activated to produce MIP-1α.

Both *cmo* (Figure 3G) and 3- to 5-month-old *Lupo* mice (% splenic weight/body weight 0.48 ± 0.02 compared to WT 0.34 ± 0.02; $P = .0003$; n = 9 mice/genotype) exhibit splenomegaly. In the case of the *cmo* mice, the splenomegaly was shown to be due to an overall increase in the numbers of hematopoietic cells, including LT-HSC, MPP, CMP, and CLP (Figure 4A) and their differentiated progeny (Figure 4B). In bone marrow, there was no change except for an increase in Mac1^{low} c-Fms^{low} c-Kit^{+} multipotent myeloid precursors. All these cells express c-Fms and/or c-Kit (CLP only express c-Kit). PSTPIP2 is tyrosine phosphorylated downstream of the CSF-1R[13,24] and c-Kit,[12] and PSTPIP2 expression increases during myeloid differentiation.[40] Furthermore, PSTPIP2 inhibits CSF-1–induced macrophage Erk1/2 activation[14] and Erk1/2 is a major regulator of CSF-1–induced proliferation in macrophages and their progenitors.[41,42] These data suggested that the extramedullary hematopoiesis was because of increased c-Kit and CSF-1R proliferation signaling. Indeed, the expansion of the splenic populations was suppressed by inhibiting c-Kit and c-Fms signaling with PLX3397 (Figures 3H and 4).

The autoinflammatory disease in PSTPIP2-deficient mice resembles human CRMO.[15] It is generally agreed that nonsteroidal anti-inflammatory drugs (NSAIDs) constitute the best initial treatment for CRMO, whereas bisphosphonates and TNFα antagonists are effective in the most severe forms.[43] However, the treatment has not been standardized. Furthermore, long-term use of NSAIDs is limited by the gastrointestinal side effects, and TNFα antagonists, although effective, increase risk of infection.[43] Based on our observations in mice, we suggest that CSF-1R and c-Kit–regulated cells of the monocytic lineage are a therapeutic target for attenuation of inflammation and osteopenia. Although effective in inhibiting the extramedullary hematopoiesis in *cmo* mice, the treatment with PLX3397 did not significantly impair bone marrow myelopoiesis or decrease the frequency of blood monocytes. These data are consistent with previous observations in CSF-1R and CSF-1–deficient mice, which indicate that the CSF-1R is not essential for many aspects of the immune defense against pathogens, other than at the maternal-fetal interface.[4,44] Thus, targeting CSF-1R and c-Kit signaling should be effective in suppressing autoinflammatory disease without impairing immunity.

Bone marrow, spleen, and peripheral blood cell populations can form OCLC in vitro in the presence of CSF-1 and RANKL.[45] Stem cell factor-induced up-regulation of the CSF-1R in c-Kit^{+} c-Fms$^{-/lo}$ Mac-1^{lo} multipotent bone marrow precursors, followed by CSF-1–stimulated RANK expression leads to the differentiation of c-Kit^{+} c-Fms^{+} Mac-1^{lo} intermediate osteoclast precursors which then further differentiate to c-Kit^{-} c-Fms^{+} Mac-1^{lo} RANK^{+} late osteoclast precursors.[8] Our results indicate that in the absence of PSTPIP2, multipotent c-Kit^{+} c-Fms^{lo} Mac-1^{lo} EOCPs are selectively increased in vivo. Furthermore, when isolated, these cells are more osteoclastogenic than their WT counterparts. Structure-function analysis reveals that PSTPIP2 regulates pathways involved in multiple steps of osteoclast differentiation, via distinct molecular interactions. The *Lupo* mutation I282N, although not being deleterious for PSTPIP2 expression, impaired the ability of PSTPIP2 to induce stable membrane invagination in COS-7 cells and in vivo leads to a very similar phenotype to the *cmo* mutation, which abolished PSTPIP2 expression. Although the conformation of PSTPIP2 in solution did not seem to be significantly affected by the I282N mutation, when expressed at high levels in COS-7 cells, PSTPIP2 I282N formed aggregates. This propensity of the *Lupo* mutant to form inactive aggregates could preferentially affect biologic processes that involve up-regulation of PSTPIP2 expression, such as the late phase of response to LPS in macrophages,[11]

myeloid differentiation,[40,46] and the function of cells that express high levels of PSTPIP2, such as osteoclasts.[14]

Targeted mutagenesis revealed that although interaction with PEST-type phosphatases was important for inhibition of TRAP expression, both the ability to interact stably with membrane phospholipids and tyrosine phosphorylation, (which presumably creates docking sites for other proteins containing phosphotyrosine-binding domains), were essential for down-regulation of TRAP expression and inhibiting subsequent OCP fusion. Although it remains to be established how membrane modeling by PSTPIP2 contributes to OC development at the molecular level, the fact that both EOCP expressing the KRQ PSTPIP2 mutant, as well as EOCP isolated from mice expressing the F-BAR domain-destabilizing *Lupo* mutation (I282N), exhibited an increased capacity to form osteoclasts in culture compared with WT counterparts, suggested that stable interaction of PSTPIP2 with the plasma membrane was important for inhibition of OC differentiation. Membrane reshaping is expected to mediate critical events during osteoclast fusion, such as the endocytosis of DC-STAMP, which is a prerequisite for high fusogenic activity,[47] and the cellocytosis, that is, cell-cell internalization events leading to plasma membrane fusion and the merging of cytoplasm between the fusion partners.[48] PSTPIP2 belongs to the FCH and BAR (F-BAR) family of proteins that have been implicated in clathrin-mediated endocytosis[10,29] and cell-to-cell fusion.[49] F-BAR proteins promote endocytosis by simultaneously interacting with membrane phospholipids, via their conserved F-BAR domains and with endocytic adaptors and dynamin, via their Src homology 3 (SH3) or muniscin C-terminal μ homology domain (μHD) domains.[10,29] PSTPIP2 lacks these domains[10] and it is tempting to speculate that it could inhibit the endocytic actions of other F-BAR proteins by competing for phospholipid binding sites without recruiting the other components of the endocytic machinery.

Interestingly, compared with WT PSTPIP2, the KRQ mutant, that had lost the ability to interact with membrane phospholipids, also exhibited a significant reduction in tyrosine phosphorylation. The requirement for membrane targeting of PSTPIP2 for efficient tyrosine phosphorylation is consistent with a previous report indicating that PSTPIP2 is a substrate of Src family kinases,[50] and with our observation that CSF-1–induced tyrosine phosphorylation of PSTPIP2 is abolished in macrophages expressing a variant of CSF-1R (CSF-1R Y559F) that is unable to recruit Src family kinases and inhibited by the Src family kinase inhibitor PP2 (data not shown). Although CSF-1 and RANKL are required for osteoclastogenesis,[6-9] our results demonstrate that CSF-1R–regulated PSTPIP2 tyrosine phosphorylation is required for suppression of osteoclastogenesis, indicating that PSTPIP2 normally plays a negative feedback role. Further investigations are necessary to determine how CSF-1R triggers the tyrosine phosphorylation of PSTPIP2 and how tyrosine phosphorylation in turn regulates PSTPIP2 activity.

The gene encoding human PSTPIP2 is located on chromosome 18q12 and mutations in this region are associated with autoimmune disorders and psychiatric disease.[51-53] Two studies of the PSTPIP2 coding region in small cohorts of patients with CRMO (n = 10) and synovitis, acne, pustulosis, hyperostosis, and osteitis (SAPHO) syndrome (n = 38)[54,55] have found rare coding region variants in PSTPIP2 that were not specifically associated with the disease. Given that the penetrance of the *cmo* and *Lupo* mutations varies greatly with the genetic background (Grosse et al[11] and data not shown), the effect of some of these mutations may have been obscured. Furthermore, as it is decreased PSTPIP2 expression that leads to disease, further investigations with larger cohorts of CRMO patients, focusing on alterations in PSTPIP2 expression are needed.

Our current and earlier[11,14] studies describe a mechanism for the development of an autoinflammatory disease affecting skin, joint, and bone, that is triggered by dysregulation of the development of myeloid cells. However, we previously demonstrated the presence of autoantibodies in PSTPIP2 deficiency disease.[11] Autoimmunity can be triggered by remnant epitopes generated after degradation of extracellular matrix components by proteases secreted by macrophages.[56] Therefore, in a broader context, a mechanism such as we describe here, involving dysregulation of the innate immune system, could contribute to the initiation of autoimmune disease. Clearly, elucidation of the molecular mechanisms underlying regulation by PSTPIP2 are highly relevant to our understanding of how genetic defects affecting early myelopoietic events predispose to chronic inflammation, bone loss and autoimmunity.

Acknowledgments

The authors thank Dr Brian West (Plexxikon, Berkeley, CA) for providing expertise on PLX3397 and its effective dosing in mice, Frank Macaluso and Leslie Gunther-Cummins (Analytical Imaging Facility at Einstein) for assistance with the electron microscopic studies, Antonios Aliprantis and the microCT core at Harvard School of Public Health, and Ranu Basu and Robin Sgueglia for technical support.

This work was supported by National Institutes of Health grant RO1 CA26504 (E.R.S.); Albert Einstein College of Medicine Cancer Center grants 5P30-CA13330 (E.R.S.) and K01AR 054486 (V.C.); a New York Community Trust Blood Diseases Grant (V.C.); and an Abbott Rheumatology Scholar Award (J.F.C.). V.N. was supported by a Fulbright award.

Authorship

Contribution: V.C. designed research, performed cytokine, osteoclast formation, and TRAP assays, FACS analysis, electron microscopy, signaling studies, generated the osteoclast cell lines, analyzed the data, and prepared the paper; V.N. performed the implant experiments and histology; J.F.C. performed the CT scan and evaluation; W.M.H. and H.T.M. performed the biochemical characterization of the *Lupo* mutation; S.N., H.K., and R.H. performed the histology and FACS analysis; M.C.N. provided expertise with CT evaluation and retroviral transduction; and E.R.S. supervised and designed the research, and prepared the paper.

Conflict-of-interest disclosure: E.R.S. has consulted for Plexxikon. The remaining authors declare no competing financial interests.

Correspondence: E. Richard Stanley, Department of Developmental and Molecular Biology, Albert Einstein College of Medicine, 1300 Morris Park Ave, Bronx, NY 10461; e-mail: richard.stanley@einstein.yu.edu; or Violeta Chitu, Department of Developmental and Molecular Biology, Albert Einstein College of Medicine, 1300 Morris Park Ave, Bronx, NY 10461; e-mail: violeta.chitu@einstein.yu.edu.

References

1. Schett G. Osteoimmunology in rheumatic diseases. *Arthritis Res Ther.* 2009;11(1):210.
2. El-Shanti H, Ferguson PJ. Chronic recurrent multifocal osteomyelitis: a concise review and genetic update. *Clin Orthop Relat Res.* 2007;462: 11-19.
3. Yasuda H, Shima N, Nakagawa N, et al. Osteoclast differentiation factor is a ligand for osteoprotegerin/osteoclastogenesis-inhibitory factor and is identical to TRANCE/RANKL. *Proc Natl Acad Sci U S A.* 1998;95(7):3597-3602.
4. Chitu V, Stanley ER. Colony-stimulating factor-1 in immunity and inflammation. *Curr Opin Immunol.* 2006;18(1):39-48.
5. Boyle JW, Simone WS, Lacey DL. Osteoclast differentiation and activation. *Nature.* 2003;423:337-342.
6. Hodge JM, Kirkland MA, Nicholson GC. Multiple roles of M-CSF in human osteoclastogenesis. *J Cell Biochem.* 2007;102(3):759-768.
7. Perkins SE, Kling SJ. Local concentrations of macrophage-stimulating factor mediate osteoclastic differentation. *Am J Physiol.* 1995;296(6 Pt 1):E1024-E1030.
8. Arai F, Miyamoto T, Ohneda O, et al. Commitment and differentiation of osteoclast precursor cells by the sequential expression of c-Fms and receptor activator of nuclear factor kappaB (RANK) receptors. *J Exp Med.* 1999;190(12):1741-1754.
9. Tanaka S, Takahashi N, Udagawa N, et al. Macrophage colony-stimulating factor is indispensable for both proliferation and differentiation of osteoclast progenitors. *J Clin Invest.* 1993;91(1): 257-263.
10. Chitu V, Stanley ER. PCH proteins, coordinators of membrane-cytoskeletal interactions. *Trends in Cell Biology.* 2007;17(3):145-156.
11. Grosse J, Chitu V, Marquardt A, et al. Mutation of mouse MAYP/PSTPIP2 causes a macrophage autoinflammatory disease. *Blood.* 2006;107(8): 3350-3358.
12. Petti F, Thelemann A, Kahler J, et al. Temporal quantitation of mutant Kit tyrosine kinase signaling attenuated by a novel thiophene kinase inhibitor OSI-930. *Mol Cancer Ther.* 2005;4(8):1186-1197.
13. Yeung YG, Soldera S, Stanley ER. A novel macrophage actin-associated protein (MAYP) is tyrosine-phosphorylated following colony stimulating factor-1 stimulation. *J Biol Chem.* 1998; 273(46):30638-30642.
14. Chitu V, Ferguson P, de Bruijn R, et al. Primed innate immunity leads to autoinflammatory disease in PSTPIP2-defcient cmo mice. *Blood.* 2009;114(12):2497-24505.
15. Ferguson PJ, Bing X, Vasef MA, et al. A missense mutation in pstpip2 is associated with the murine autoinflammatory disorder chronic multifocal osteomyelitis. *Bone.* 2006;38(1):41-47.
16. Ferguson PJ, El-Shanti H. Autoinflammatory bone disorders. *Curr Opin Rheumatol.* 2007; 19(5):492-498.
17. Hentunen T, Choi S, Boyce B, et al. A murine model of inflammatory bone disease. *Bone.* 2000; 26(2):183-188.
18. Nandi S, Akhter MP, Seifert MF, Dai XM, Stanley ER. Developmental and functional significance of the CSF-1 proteoglycan chondroitin sulfate chain. *Blood.* 2005;107(2):786-795.
19. Dai XM, Zong XH, Akhter MP, Stanley ER. Osteoclast deficiency results in disorganized matrix, reduced mineralization, and abnormal osteoblast behavior in developing bone. *J Bone Miner Res.* 2004;19(9):1441-1451.
20. Chitu V, Yeung YG, Yu W, Stanley ER. Measurement of macrophage growth and differentiation. In Coligan JE, Bierer BE, Marguiles DH, Strober W, eds. *Current Protocols in Immunology.* John Wiley and Sons. Somerset, NJ. 2011;92: 14.20.11-14.20.26.
21. Faccio R, Zou W, Colaianni G, Teitelbaum SL, Ross FP. High dose M-CSF partially rescues the Dap12−/− osteoclast phenotype. *J Cell Biochem.* 2003;90(5):871-883.
22. Kara FM, Chitu V, Sloan J, et al. Adenosine A1R play a critical role in osteoclast formation and function. *FASEB J.* 2010;24(7):2325-2333.
23. Tintut Y, Parhami F, Tsingotjidou A, Tetradis S, Territo M, Demer LL. 8-Isoprostaglandin E2 enhances receptor-activated NFkappa B ligand (RANKL)-dependent osteoclastic potential of marrow hematopoietic precursors via the cAMP pathway. *J Biol Chem.* 2002;277(16):14221-14226.
24. Chitu V, Pixley FJ, Macaluso F, et al. The PCH family member MAYP/PSTPIP2 directly regulates F-actin bundling and enhances filopodia formation and motility in macrophages. *Mol Biol Cell.* 2005;16(6):2947-2959.
25. Boyce BF, Yoneda T, Lowe C, Soriano P, Mundy GR. Requirement of pp60c-src expression for osteoclasts to form ruffled borders and resorb bone in mice. *J Clin Invest.* 1992;90(4):1622-1627.
26. Zsebo KM, Wypych J, McNiece IK, et al. Identification, purification, and biological characterization of hematopoietic stem cell factor from buffalo rat liver-conditioned medium. *Cell.* 1990;63(1): 195-201.
27. DeNardo DG, Brennan DJ, Rexhepaj E, et al. Leukocyte complexity predicts breast cancer survival and functionally regulates response to chemotherapy. *Cancer Discov.* 2011;1(1):54-67.
28. Tsujita K, Suetsugu S, Sasaki N, Furutani M, Oikawa T, Takenawa T. Coordination between the actin cytoskeleton and membrane deformation by a novel membrane tubulation domain of PCH proteins is involved in endocytosis. *J Cell Biol.* 2006; 172(2):269-279.
29. Henne WM, Boucrot E, Meinecke M, et al. FCHo proteins are nucleators of clathrin-mediated endocytosis. *Science.* 2010;328(5983):1281-1284.
30. Shimada A, Niwa H, Tsujita K, et al. Curved EFC/F-BAR-domain dimers are joined end to end into a filament for membrane invagination in endocytosis. *Cell.* 2007;129(4):761-772.
31. Peter B, Kent H, Mills I, et al. BAR domains as sensors of membrane curvature: the amphiphysin BAR structure. *Science.* 2004;303(5657):495-499.
32. Arron JR, Choi Y. Bone versus immune system. *Nature.* 2000;408(6812):535-536.
33. Walsh MC, Kim N, Kadono Y, et al. Osteoimmunology: interplay between the immune system and bone metabolism. *Annu Rev Immunol.* 2006; 24:33-63.
34. Wei S, Lightwood D, Ladyman H, et al. Modulation of CSF-1-regulated post-natal development with anti-CSF-1 antibody. *Immnobiology.* 2005; 210(2-4):109-119.
35. Clarke B. Normal Bone Anatomy and Physiology. *Clin J Am Soc Nephrol.* 2008;3(Suppl 3):S131-S139.
36. Yu X, Huang Y, Collin-Osdoby P, Osdoby P. CCR1 chemokines promote the chemotactic recruitment, RANKL development, and motility of osteoclasts and are induced by inflammatory cytokines in osteoblasts. *J Bone Miner Res.* 2004; 19(12):2065-2077.
37. Oba Y, Lee JW, Ehrlich LA, et al. MIP-1alpha utilizes both CCR1 and CCR5 to induce osteoclast formation and increase adhesion of myeloma cells to marrow stromal cells. *Exp Hematol.* 2005; 33(3):272-278.
38. Broxmeyer HE, Cooper S, Hangoc G, Gao JL, Murphy PM. Dominant myelopoietic effector functions mediated by chemokine receptor CCR1. *J Exp Med.* 1999;189(12):1987-1992.
39. Vallet S, Raje N, Ishitsuka K, et al. MLN3897, a novel CCR1 inhibitor, impairs osteoclastogenesis and inhibits the interaction of multiple myeloma cells and osteoclasts. *Blood.* 2007;110(10):3744-3752.
40. Ivanova N, Dimos J, Schaniel C, Hackney J, Moore K, Lemischka I. A stem cell molecular signature. *Science.* 2002;298(5593):601-604.
41. Yu W, Chen J, Xiong Y, Pixley FJ, Yeung YG, Stanley ER. Macrophage proliferation is regulated through CSF-1 receptor tyrosines 544, 559, and 807. *J Biol Chem.* 2012;287(17):13694-13704.
42. Takeshita S, Faccio R, Chappel J, et al. c-Fms tyrosine 559 is a major mediator of M-CSF-induced proliferation of primary macrophages. *J Biol Chem.* 2007;282(26):18980-18990.
43. Wipff J, Adamsbaum C, Kahan A, Job-Deslandre C. Chronic recurrent multifocal osteomyelitis. *Joint Bone Spine.* 2011;78(6):555-560.
44. Guleria I, Pollard JW. The trophoblast is a component of the innate immune system during pregnancy. *Nat Med.* 2000;6(5):589-593.
45. Teitelbaum SL. Bone resorption by osteoclasts. *Science.* 2000;289(5484):1504-1508.
46. Brown A, Wilkinson C, Waterman S, et al. Genetic regulators of myelopoiesis and leukemic signaling identified by gene profiling and linear modeling. *J Leukoc Biol.* 2006;80(2):430-447.
47. Mensah KA, Ritchlin CT, Schwarz EM. RANKL induces heterogeneous DC-STAMPlo and DC-STAMPhi osteoclast precursors of which the DC-STAMPlo precursors are the master fusogens. *J Cell Physiol.* 2010;223(1):76-83.
48. Vignery A. Macrophage fusion: the making of osteoclasts and giant cells. *J Exp Med.* 2005; 202(3):337-340.
49. Richard JP, Leikina E, Langen R, et al. Intracellular curvature-generating proteins in cell-to-cell fusion. *Biochem J.* 2011;440(2):185-193.
50. Wu Y, Dowbenko D, Lasky LA. PSTPIP 2, a second tyrosine phosphorylated, cytoskeletal-associated protein that binds a PEST-type protein-tyrosine phosphatase. *J Biol Chem.* 1998; 273(46):30487-30496.
51. Merriman T, Cordell H, Eaves I, et al. Suggestive evidence for association of human chromosome 18q12-q21 and its orthologue on rat and mouse chromosome 18 with several autoimmune diseases. *Diabetes.* 2001;50(1):184-194.
52. Pickard B, Malloy P, Clark L, et al. Candidate psychiatric illness genes identified in pacients with pericentric inversions of chromosome 18. *Psychiatric Genetics.* 2005;15:37-44.
53. Golla A, Jansson A, Ramser J, et al. Chronic recurrent multifocal osteomyelitis (CRMO): evidence for a susceptibility gene located on chromosome 18q21.3-18q22. *Eur J Hum Genet.* 2002;10(3):217-221.
54. Jansson A, Renner E, Ramser J, et al. Classification of non-bacterial oteitis: retrospective study of clinical, immunological and genetic aspects in 89 patients. *Rheumatology.* 2007;46(1):154-160.
55. Hurtado-Nedelec M, Chollet-Martin S, Chapeton D, Hugot JP, Hayem G, Gérard B. Genetic susceptibility factors in a cohort of 38 patients with SAPHO syndrome: a study of PSTPIP2, NOD2, and LPIN2 genes. *J Rheumatol.* 2010;37(2):401-409.
56. Descamps FJ, Van den Steen PE, Nelissen I, Van Damme J, Opdenakker G. Remnant epitopes generate autoimmunity: from rheumatoid arthritis and multiple sclerosis to diabetes. *Adv Exp Med Biol.* 2003;535:69-77.

Supplemental material

PSTPIP2 deficiency in mice causes osteopenia and increased differentiation of multipotent myeloid precursors into osteoclasts

Violeta Chitu, Viorel Nacu, Julia F. Charles, William M. Henne, Harvey T. McMahon, Sayan Nandi, Halley Ketchum, Renee Harris, Mary C. Nakamura, E. Richard Stanley

Fig. S1. The accelerated osteoclast differentiation in BM cultures of PSTPIP2-deficient *cmo* mice is not due to an increased frequency of osteoclast precursors. (A) Frequency of c-Kit^{+} Mac-1^{low} OCP in the bone marrow of wt and *cmo* mice, n ≥ 7mice. (B) Bone marrow cells of wt and *cmo* mice were grown in CSF-1 and RANKL for the indicated times, fixed and stained for TRAP. (C) Quantification of TRAP^{+} cells with more than 3 nuclei (osteoclast-like cells, OCLC, n ≥ 3 independent experiments. (D) Dentine resorption in day 6 osteoclast cultures. (E) Quantification of the areas of the dentine resorption pits, average of triplicate cultures from 3 mice/genotype. Data ± S.E.M., *, significantly different from wt, $p < 0.05$.

Chitu et al. Fig. S1.

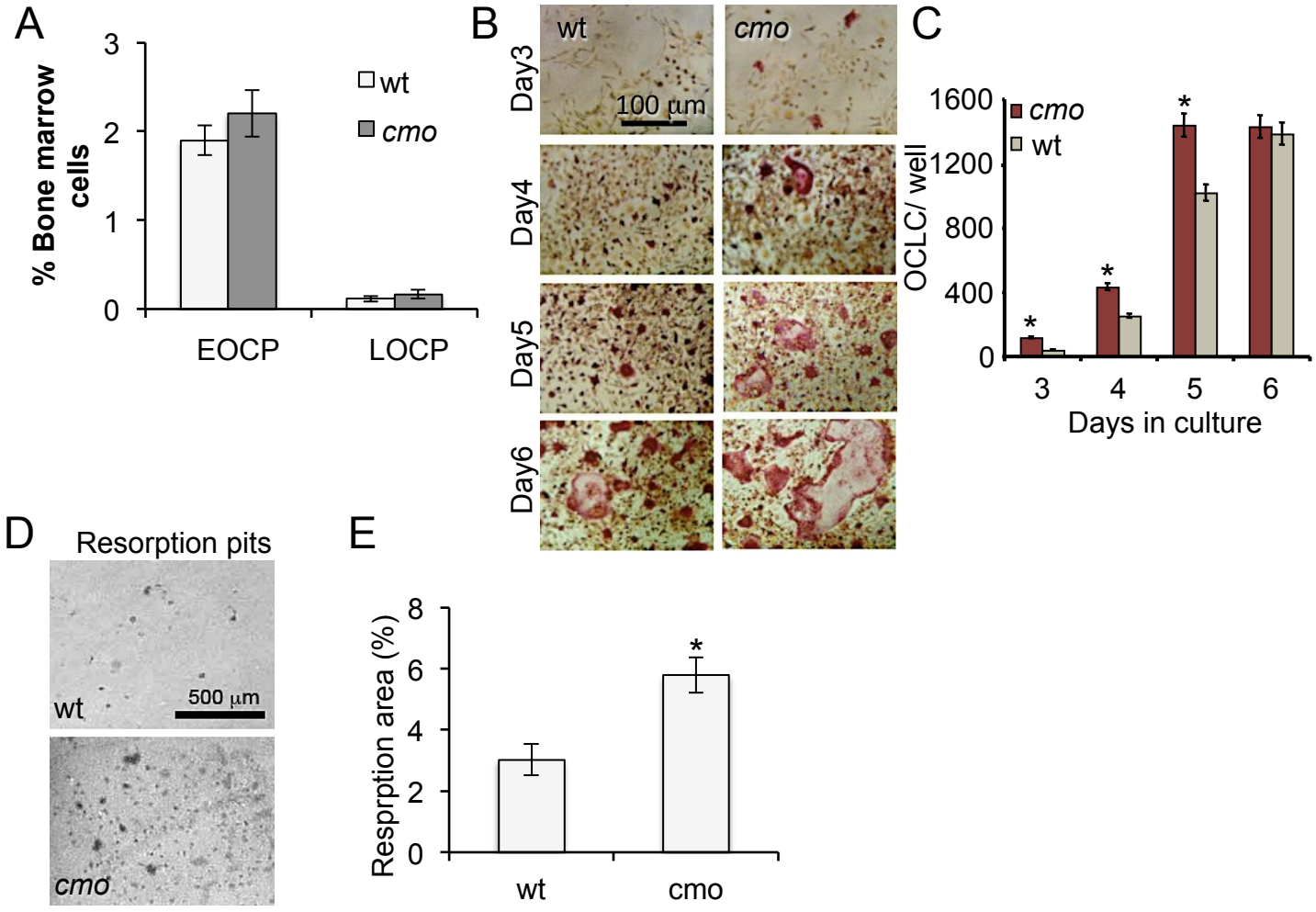

Fig. S2. Effects of the *Lupo* mutation (I282N) on PSTPIP2 folding (A) Modeling of the effect of the *Lupo* mutation, based on the crystal structure of the closely related F-BAR protein, FCHo2. Upper panel, the FCHo2 F-BAR dimer (pdb: 2V0o), with one monomer as a ribbon model and the other as a surface model with the hydrophobic residues shown in green. Lower panel (boxed region in upper panel), FCHo2 and PSTPIP2 alignments indicate that FCHo2 residue Ile-268 (indicated by the red arrow) is equivalent to PSTPIP2 I282. The I282N mutation is predicted to dislodge the unstructured C-terminus out of the hydrophobic cleft along the adjacent monomer, and thus destabilize F-BAR dimerization in this region. (B) Analysis of recombinant PSTPIP2 in solution by circular dichroism indicates that it adopts an alpha-helical structure, evidenced by the dramatic dip in delta e (ellipticity). Substitution of Ile-282 with Asn slightly affects the helical formation, but PSTPIP2 remains in a mostly folded state in solution. A.U., absorbance units.

Chitu et al. Fig. S2.